

AD-A095 359

AEROSPACE CORP EL SEGUNDO CA INFORMATION PROCESSING DIV F/G 20/4

THE AEROSPACE THERMAL MODEL (HFLUX)--ITS STRUCTURE AND UTILITY.(U)

DEC 80 J K DODD

F04701-80-C-0081

UNCLASSIFIED

TR-0081(6638-05)-1

SD-TR-80-81

NL

1 1 1
201
1 1 1



END
DATE
FILMED
3 8
DTIC

AD A095359

The Aerospace Thermal Model (RFLUX) - Its Structure and Utility

LEVEL II

Prepared by
J. K. DODD
Engineering Data Systems Department
Information Processing Division
The Aerospace Corporation
El Segundo, Calif. 90245

DTIC
ELECTE
FEB 23 1980
S D

1 December 1980

Interim Report

APPROVED FOR PUBLIC RELEASE;
DISTRIBUTION UNLIMITED

Prepared for
AIR FORCE TECHNICAL APPLICATIONS CENTER
Patrick Air Force Base, Fla. 32920

SPACE DIVISION
AIR FORCE SYSTEMS COMMAND
Los Angeles Air Force Station
P.O. Box 92960, Worldway Postal Center
Los Angeles, Calif. 90009

DOC FILE COPY

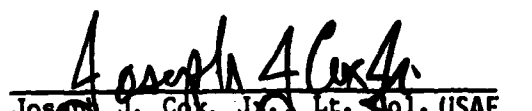
81 2 23 083

This interim report was submitted by The Aerospace Corporation, El Segundo, CA 90245, under Contract No. F04701-80-C-0081 with the Space Division, P.O. Box 92960, Worldway Postal Center, Los Angeles, CA 90009. It was reviewed and approved for The Aerospace Corporation by W. R. Warren, Jr., Director, Aerophysics Laboratory. Lieutenant James C. Garcia, SD/YLXT, was the project officer for Mission-Oriented Investigation and Experimentation (MOIE) Programs.

This report has been reviewed by the Public Affairs Office (PAS) and is releasable to the National Technical Information Service (NTIS). At NTIS, it will be available to the general public, including foreign nations.

This technical report has been reviewed and is approved for publication. Publication of this report does not constitute Air Force approval of the report's findings or conclusions. It is published only for the exchange and stimulation of ideas.


James C. Garcia, Lt, USAF
Project Officer


Joseph G. Cook, Jr., Lt. Col. USAF
Chief, Advanced Technology Division

FOR THE COMMANDER


Burton H. Holaday, Col., USAF
Directorate of Space Systems Planning
Deputy for Technology

UNCLASSIFIED

SECURITY CLASSIFICATION OF THIS PAGE (When Data Entered)

19 REPORT DOCUMENTATION PAGE		READ INSTRUCTIONS BEFORE COMPLETING FORM
1. REPORT NUMBER SD-TR-80-81	2. GOVT ACCESSION NO. AD-A095359	3. RECIPIENT'S CATALOG NUMBER
6. TITLE (and Subtitle) THE AEROSPACE THERMAL MODEL (HFLUX)--Its Structure and Utility.	9. Interim rept.	5. TYPE OF REPORT & PERIOD COVERED
7. AUTHOR(s) Joseph K. Dodd	14. TR-0081(6638-05)-1	PERFORMING ORG. REPORT NUMBER
	15. F04701-80-C-0081	CONTRACT OR GRANT NUMBER(s)
9. PERFORMING ORGANIZATION NAME AND ADDRESS The Aerospace Corporation El Segundo, Calif. 90045		10. PROGRAM ELEMENT, PROJECT, TASK AREA & WORK UNIT NUMBERS
11. CONTROLLING OFFICE NAME AND ADDRESS Air Force Technical Applications Center Patrick Air Force Base, Fla. 32935	11. 1 December 1980	12. REPORT DATE
14. MONITORING AGENCY NAME & ADDRESS (if different from Controlling Office) Space Division Air Force Systems Command Los Angeles, Calif. 90009	12. 29	13. NUMBER OF PAGES 24
		15. SECURITY CLASS. (of this report) Unclassified
		15a. DECLASSIFICATION/DOWNGRADING SCHEDULE
16. DISTRIBUTION STATEMENT (of this Report) Approved for public release; distribution unlimited.		
17. DISTRIBUTION STATEMENT (of the abstract entered in Block 20, if different from Report)		
18. SUPPLEMENTARY NOTES		
19. KEY WORDS (Continue on reverse side if necessary and identify by block number) Thermal Modeling Boundary Layer Meteorology Infrared Remote Sensing		
20. ABSTRACT (Continue on reverse side if necessary and identify by block number) A one-dimensional model of the boundary layer (HFLUX) developed at Penn State by Carlson and Boland to simulate the behavior of the ground temperature over complex terrain has been modified by The Aerospace Corporation for use in several field experiments that require the accurate prediction of the surface radiometric temperature as a function of surface (thermal inertia, albedo, and moisture availability) and meteorological (stability and wind speed) parameters. HFLUX has demonstrated its utility for use with a broad class of remote thermal		

DD FORM 1473
(FACSIMILE)UNCLASSIFIED 409525
SECURITY CLASSIFICATION OF THIS PAGE (When Data Entered)

UNCLASSIFIED

SECURITY CLASSIFICATION OF THIS PAGE(When Data Entered)

19. KEY WORDS (Continued)

20. ABSTRACT (Continued)

imaging problems. The physical principles upon which the model is structured, a discussion of recent work with the Aerospace model, and future developmental objectives are included in this report.

UNCLASSIFIED

SECURITY CLASSIFICATION OF THIS PAGE(When Data Entered)

CONTENTS

I.	INTRODUCTION.....	5
II.	MODEL STRUCTURE.....	7
III.	MODEL CAPABILITIES DEVELOPED AT AEROSPACE.....	23
	A. Dual-Mode Calculations.....	23
	B. Subsurface Model.....	23
	C. Dynamic Updating.....	24
IV.	FUTURE DEVELOPMENTS.....	25
	A. Soil Moisture.....	25
	B. Energy Budget Over Water.....	26
	C. Model Consolidation.....	26
	REFERENCES	27

Accession For	
NTIS GRA&I	<input checked="" type="checkbox"/>
DTIC TAB	<input type="checkbox"/>
Unannounced	<input type="checkbox"/>
Justification	
By _____	
Distribution/ _____	
Availability Codes	
Dist	Avail and/or Special
A	

FIGURES

1.	Basic Structure of Model.....	8
2.	Energy Balance at Earth-Atmosphere Interface.....	10
3.	Flow Chart of Model Solution Sequence from Time t_0 to $t_0 + \Delta t$	15
4.	Basic Structure of Nocturnal Component of Model.....	19
5.	Schematic of Initial Wind and Temperature Profiles for Nocturnal Component of Model.....	21

I. INTRODUCTION

The interpretation of thermal infrared (IR) images generated from aircraft or satellite sensor data requires an understanding of the surface and atmospheric parameters that determine the thermal response of the ground to the incident solar insolation. A well-constituted physical model that accurately simulates the energy balance at the earth-atmosphere interface is an indispensable analysis tool for use in the identification of surface parameters that cause horizontal signature differences. For example, if independent measurements of surface shortwave albedo and local meteorological variables are available, successive iterations of a thermal model executed over a range of various values for ground conductivity can be registered with a background temperature image produced from IR measurements to infer the horizontal distribution of the thermal conductivity of the soil. This information can be used to determine the geologic surface materials distributed across a large image scene. In a similar manner, soil moisture and anthropogenic or geothermal heat sources can be inferred.

For use in background modeling applications, a modified version of the boundary-layer model (HFLUX), developed by Carlson and Boland¹ for simulation of the behavior of ground temperature over complex terrain, is being implemented at The Aerospace Corporation. The model can be used in various field experiments that require accurate prediction of the surface radiometric temperature.

II. MODEL STRUCTURE

The model represents the physics of the response of the ground to the solar forcing by the use of Monin-Obukov theory with an implicit K-type parameterization for the eddy fluxes of heat, moisture, and momentum in the surface layer. The primary forcing mechanism is the net radiation, but the partitioning of the energy balance into the ground heat flux and the latent and sensible heat fluxes into the atmosphere is determined by the substrate and atmospheric variables. Solutions are obtained as successive equilibrium states of the energy balance controlled by similarity theory in the surface layer and the temperature diffusion equation in the soil. Typically, the model is integrated to simulate a complete diurnal cycle over which the terrain parameters and the temperature at the bottom of the substrate slab are held constant. Horizontal advection is not included in the model.

A schematic view of HFLUX is presented in Fig. 1. The substrate slab is of variable depth with a user-defined number of levels, permitting coarse or detailed representations of the subsurface thermal parameters. The surface air layer depth is fixed at 50 m, with a 1-cm transition layer at the earth's surface that contains both molecular and eddy heat conduction.* Within this transitional sublayer, the fluxes of moisture and heat are assumed to be independent of the stability. A well-mixed layer is represented in bulk form above the surface layer and its depth, H , is governed by a formulation presented by Tennekes² in which H grows throughout the day as a result of the surface heat flux from below and entrainment of air with a higher potential temperature from above. The atmosphere above the surface layer is modeled differently at night; the structure of the nocturnal boundary layer is described later in this section.

The solution sequence begins with the net radiation given by the surface energy balance

*The exact depth of the transition layer is inconsequential insofar as the surface temperature determination is concerned.

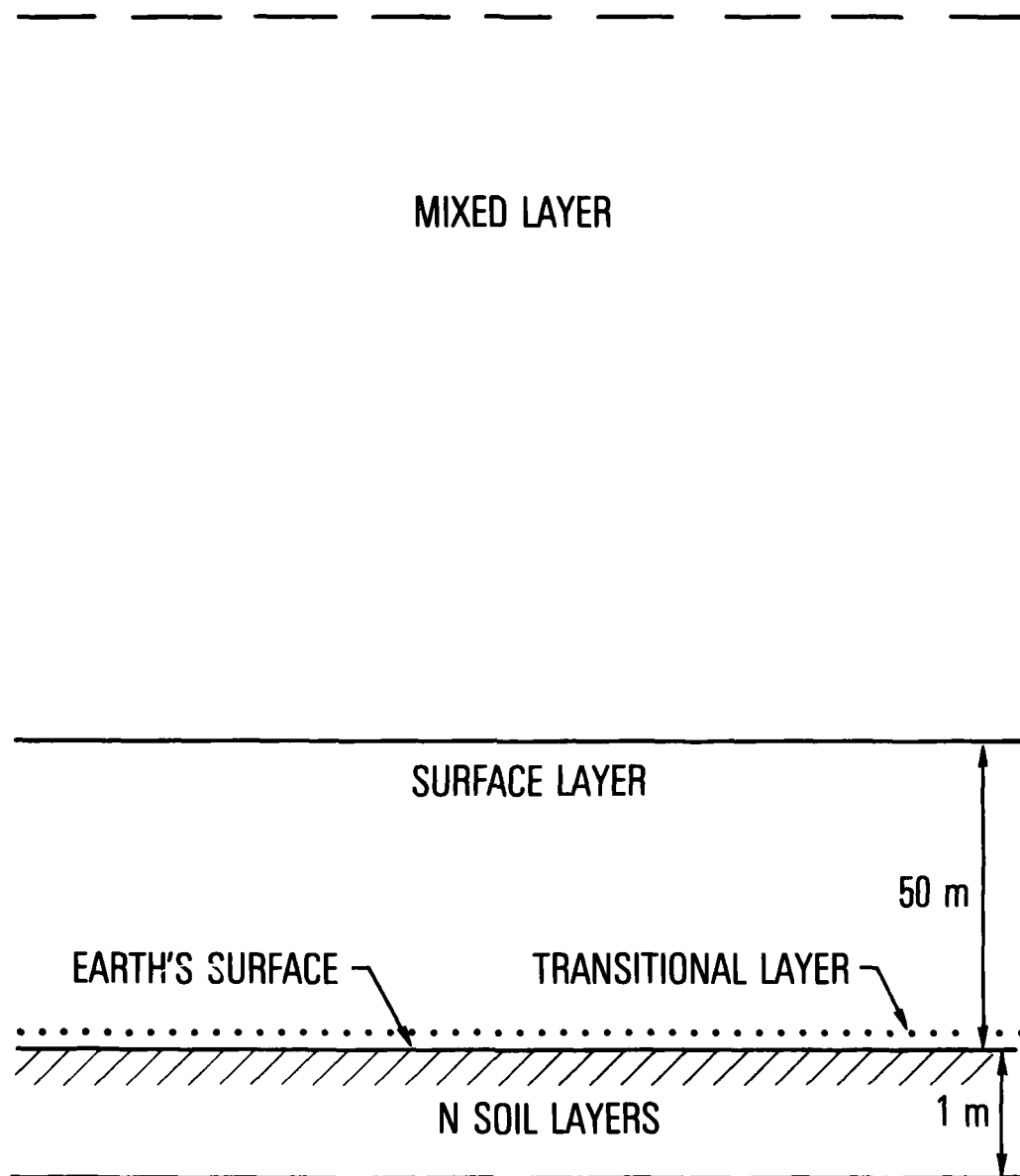


Fig. 1. Basic Structure of Model

$$R_N = G_o + H_o + E_o \quad (1)$$

where G_o , H_o , and E_o represent the heat flux into the ground, the sensible heat flux into the atmosphere, and the latent heat flux into the atmosphere. All quantities are positive when directed away from the surface. The net radiation is actually calculated from the radiative fluxes at the surface

$$R_N = S + F_d - F_u \quad (2)$$

where S is the solar flux at the surface and F_d and F_u are the upward and downward terrestrial fluxes, respectively. Figure 2 is a schematic of the energy balance that shows the direction of the fluxes at midday. Total downwelling irradiance absorbed at the surface, S , is calculated from a one-layer radiative transfer model. S is a function of solar geometry, atmospheric transmission coefficients, and ground albedo, A_o , determined as

$$S = S^* \frac{(1 - A_o)}{1 - XA_o} \quad (3)$$

where S^* and X are general transmission relations containing the solar constant and coefficients for dust, water vapor, air molecules, ozone, and clouds. S can be calculated for sloping terrain of arbitrary orientation. The upward and downward directed fluxes of longwave terrestrial radiation are given as

$$F = \epsilon_g \sigma T_g^4 \quad (4)$$

$$F_d = \epsilon_A \sigma T_A^4 \quad (5)$$

where σ is the Boltzmann constant, and ϵ_g and ϵ_A are the emissivities for the ground and atmosphere. Most surface materials have values of ϵ_g that are between 0.9 and 1, and ϵ_A is a function of the water vapor mixing ratio in the surface layer.

$$SW \downarrow + IR \downarrow - IR \uparrow = E \uparrow + H \uparrow + G \downarrow \text{ WHERE:}$$

$SW \downarrow$ = SOLAR RADIATION

$IR \downarrow$ = ATMOSPHERIC INFRARED RADIATION

$IR \uparrow$ = SURFACE INFRARED RADIATION

$E \uparrow$ = LATENT HEAT FLUX

$H \uparrow$ = SENSIBLE HEAT FLUX

$G \downarrow$ = GROUND HEAT FLUX

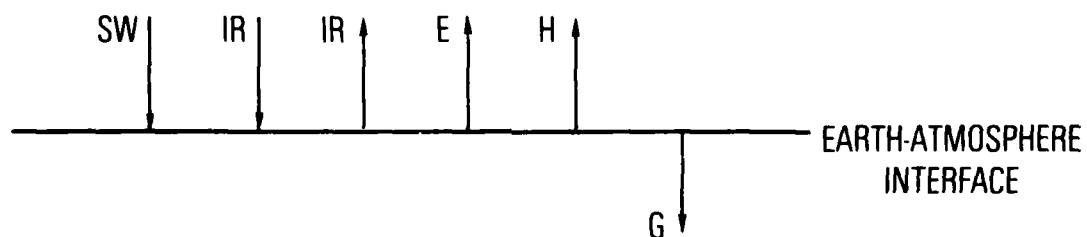


Fig. 2. Energy Balance at Earth-Atmosphere Interface

The surface fluxes of sensible and latent heat are parameterized in terms of eddy and molecular diffusivities as

$$H_o = -(C_s + \rho c_p K_H) \frac{\partial \theta}{\partial z} \quad (6)$$

$$E_o = -\left(\frac{L_E}{c_p} C_w + \rho L_E K_q\right) \frac{\partial q}{\partial z} \quad (7)$$

where C_s and C_w are the molecular diffusivities for heat and water vapor, q , L_E is the latent heat of vaporization, and K_H and K_q are the eddy diffusivities for heat and water vapor, which are assumed to be equal. The sensible and evaporative heat fluxes at the surface are calculated by integrating Eqs. (6) and (7) from $Z = 0$ to the top of the surface layer, Z_A

$$H_o = \frac{\rho C_p}{I} (\theta_o - \theta_A) \quad (8)$$

$$E_o = \frac{\rho L_E}{I} M (q_{os} - q_o) \quad (9)$$

where q_{os} is the surface saturation mixing ratio, q_A is the mixing ratio at Z_A , and M is the moisture availability parameter described by Nappo.³ Values of M range from 0 to 1 and represent a fraction of the potential evaporation rate for a saturated surface. As such, the factor M accounts for the reduction in the efficiency of evaporation caused by subsaturation of the surface. Evaporation is set to zero at night when $q_A > q_{os}$.

In Eq. (8), I is essentially the vertical integral of the inverse of the diffusivities

$$I = \int_0^{Z_A} \frac{dz}{K_H + C_s / \rho c_p} = I_1 + I_2 \quad (10)$$

This integral is calculated in two sections: from $z = 0$ to Z_l , which is the depth of the transitional layer over which molecular conduction dominates the transfer process, and from Z_l to Z_a , where C_s and C_w are assumed to be negligible compared with $\rho c_p K_H$. Thus, turbulent eddy conduction determines the exchange in evaluating the expression I_2 . The term ku_*z/ϕ_h is substituted for K_H where u_* is given by

$$u_* = \frac{\bar{u}_A k}{\int_{Z_0}^{Z_A} \phi_m(z)/z(dz)} \quad (11)$$

and u_A is the wind speed at Z_A , k is von Karman's constant (0.4), and Z_0 is the roughness length. The parameter u_* reflects the magnitude of mechanically produced turbulence. The functional forms for ϕ_H and ϕ_M have been given by Panofsky.⁴

The ground heat flux is given by the standard conduction equation

$$G_o = \frac{\lambda(T_o - T_{-1})}{\Delta z} \quad (12)$$

where λ is the thermal conductivity of the substrate and T_{-1} is the temperature at the first soil level below the surface. The transfer of heat through the soil is governed by the diffusion equation

$$\frac{\partial T}{\partial t} = \kappa \frac{\partial^2 T}{\partial z^2} \quad (13)$$

where κ is the thermal diffusivity of the substrate and is equivalent to λ/C_g , where C_g is the ground heat capacity.

The diffusivity and conductivity can be combined to form a parameter called the thermal inertia, P , where

$$P = \frac{\lambda}{\kappa}^{1/2} \quad (14)$$

is a measure of the rate of heat transfer at the interface between the ground and atmosphere. Sensitivity tests indicate that whereas model solutions depend on the value of P independently of the choices λ and κ , λ and κ must not be chosen completely independent of one another. Values of λ and κ cited in the literature appear to vary systematically for a wide variety of real materials. Accordingly, 20 pairs of λ and κ based on values reported in the Manual of Remote Sensing⁵ and by Sellers⁶ have been assembled to produce a regression equation whereby specification of P will determine uniquely a λ , κ pair. Thus, it was found that

$$\lambda = -0.00013 + 0.0502P + 1.21P^2 \quad (15)$$

where

$$\kappa = \frac{\lambda^2}{P^2} \quad (16)$$

Equation (15) explains 91% of the variance of λ about P and provides an empirical result that, for most types of materials, realistically represents the physical relationship of λ and κ to P . The regression Eq.(15) corresponds to a diverse range of soil types (pumice to quartzite).

Equations (8), (9), and (12) can be combined with the energy balance [Eq. (1)] to form an expression for the sensible heat flux at the surface

$$H_o = \frac{R_N - f(\bar{u}_A)M(q_{os} - q_A) - A}{1 + DI} \quad (17)$$

in which

$$A = \frac{\lambda(\Gamma Z_A + T_o - T_{-1})}{\Delta z} \quad (17a)$$

$$D = \frac{\lambda}{\Delta z \rho c_p} \quad (17b)$$

where Γ is the dry adiabatic lapse rate, and $f(u_A)$ is $\rho L_E/I$.

The ground temperature, T_o , is determined by equating the right-hand sides of Eqs. (1) and (2), which produces the quartic equation

$$AT_o^4 + BT_o + C = 0 \quad (18)$$

where

$$A = \epsilon_g \sigma \quad (18a)$$

$$B = \frac{\lambda}{\Delta z} \quad (18b)$$

and

$$C = S + \lambda \frac{T-1}{\Delta z} - \epsilon_A \sigma T_A^4 - H_o - E_o \quad (18c)$$

At each time step, Newton's technique for finding real zeros of a polynomial is iterated until Eq. (18) converges to the correct value for T_o . At night, in the nonturbulent surface layer, H_o , E_o , and S are zero so that Eq. (18) expresses a balance between the longwave terrestrial radiation and the ground heat flux. As such, the value of the thermal inertia, P , is an important determinant in the nighttime behavior of T_o .

This series of equations is cycled through for convergence. One iteration per time step of 4 min has been found sufficient to ensure accurate solutions. The flow chart, Fig. 3, schematically traces the order of calculation; the sequence ends with the determination of the temperature profile in the soil at the next time step from which the model integration time is incremented, and the cycle is repeated. The temperature profile in the surface layer and substrate, as well as the surface radiative and turbulent energy fluxes, are all part of the solution set.

The nighttime mode of calculation requires a different methodology, because the physics driving the surface layer are quite dissimilar from those of the daytime. During the day, the net radiation is the forcing mechanism, and the heat flux component is a function of the moisture availability and thermal

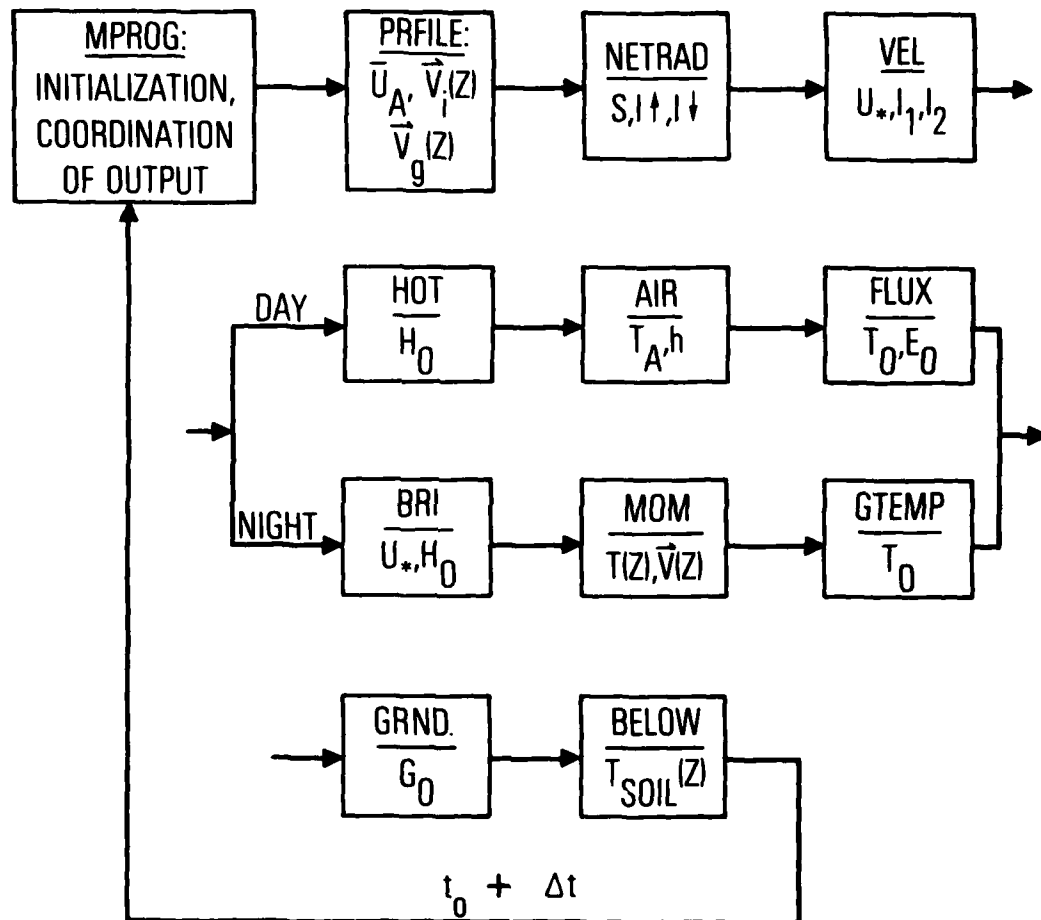


Fig. 3. Flow Chart of Model Solution Sequence from Time t_0 to $t_0 + \Delta t$

inertia. The surface layer is then unstable and the heat flux determines the stability. Near sunset, the upward heat flux vanishes and the radiational cooling causes the ground temperature to decrease rapidly; subsequently, the heat flux changes sign and becomes passively dependent on the lapse rate near the ground. To account for this, a modified form of a scheme proposed by Blackadar⁷ has been incorporated into the model. The maintenance of turbulence at night is calculated as a function of the bulk Richardson number, B , in the surface layer. The value of B determines the form of the profile equations and is given by

$$B = \frac{g}{\bar{\theta}} \frac{Z_A}{W_A} \left[(\theta_A - \theta_1) + T_* \ln \frac{Z_A}{Z_0} \right] \quad (19)$$

where g is the acceleration caused by gravity, $\bar{\theta}$ is an average temperature in the surface layer, θ_A is the potential temperature at Z_A , W_A is the magnitude of the wind at Z_A , and θ_1 is a "shelter" height temperature provided by a prognostic equation relating radiational convergence and turbulent flux convergence

$$\frac{\partial \theta_1}{\partial t} = A(\theta_g - \theta_1) + B \frac{H_0}{\rho c_p Z_1} \quad (20)$$

in which A and B have been empirically determined as $8.3 \times 10^{-4} s^{-1}$ and 0.2 , respectively. Monin-Obukov scaling is used to obtain T_* , u_* , and the surface heat flux, H_0 . Thus

$$T_* = \frac{\theta_A - \theta_1}{\ln Z_1/Z_A - \psi_h} \quad (21)$$

$$u_* = \frac{k W_A}{\ln Z_1/Z_0 - \psi_m} \quad (22)$$

$$H_0 = -k \rho c_p u_* T_* \quad (23)$$

where Z_0 is the roughness length, ψ_h and ψ_m are the nondimensional profiles for temperature and wind, the functional forms of which are dependent on stability, and W_A is the magnitude of the wind vector at a height Z_A (50 m). The vertical profiles for temperature and wind are provided through the integration of the U, V momentum equations and the thermodynamic equation

$$\frac{\partial U_i}{\partial t} = f(V_i - V_{gi}) + \frac{K_{mi} + 1}{\Delta z^2} (U_{i+1} - U_i) - \frac{K_{mi}}{\Delta z^2} (U_i - U_{i-1}) \quad (24)$$

$$\frac{\partial V_i}{\partial t} = -f(U_i - U_{gi}) + \frac{K_{mi} + 1}{\Delta z^2} (V_{i+1} - V_i) - \frac{K_{mi}}{\Delta z^2} (V_i - V_{i-1}) \quad (25)$$

$$\frac{\partial \theta_i}{\partial t} = \frac{K_{Hi} + 1}{\Delta z^2} (\theta_{i+1} - \theta_i) - \frac{K_{Hi}}{\Delta z^2} (\theta_i - \theta_{i-1}) \quad (26)$$

where f is the Coriolis parameter and Δz is a layer depth of 50 m. Horizontal advection has not been included in the model. The eddy exchange coefficients for momentum and heat, K_M and K_H , are assumed equal in the stable nocturnal boundary layer and are given by a form proposed by Mellor and Yamada⁸, with the use of boundary layer data and second order closure

$$K_i = l^2 S_i \left(\frac{Rc_i - R_i}{Rc_i} \right) \quad (27)$$

where

$$S_i = \frac{[(U_i - U_{i-1})^2 + (V_i - V_{i-1})^2]^{1/2}}{\Delta z} \quad (28)$$

and l scales as kz (taken to be 28 m) in the surface layer. The local Richardson number is calculated as

$$R_i = \frac{g}{\theta \Delta z} \frac{(\theta_i - \theta_{i-1})}{S_i^2} \quad (29)$$

and the critical Richardson number is calculated as a function of the geostrophic wind with the use of an empirical result given by Vigeant⁹

$$Rc_i = 0.5542 e^{-[0.2129(U_{gi}^2 + V_{gi}^2)^{1/2}] + 0.2} \quad (30)$$

When the local Richardson number exceeds the critical value, turbulent exchange ceases at that height and K is arbitrarily set equal to zero.

The lowest layer must be treated differently, because there is no turbulent exchange through the underlying surface. The last terms in Eqs. (24) through (26) must be replaced by $-u_*^2 U_1 / W_A \Delta z$, $-u_*^2 V_1 / W_A \Delta z$, and $-H_o / c_p \rho \Delta z$, respectively.

The integration is performed over a 1000-m-deep layer consisting of 20 equally spaced intervals ($i = 1, 20$) 50 m apart (Fig. 4) and is begun in the late afternoon or evening when the surface heat flux has changed sign. Forward differencing is used, and a time step of 120 sec has been found adequate to ensure computational stability.

Initially, the 1000-m layer is assumed to be well mixed, and the vertical distribution of θ is set equal to a constant θ_A at the time of the stability reversal, which is reasonable for late afternoon on a sunny day. The vertical shear of the geostrophic wind is determined from an analysis of local surface fields of temperature and pressure; usually only one or two additional wind observations above the surface layer are available. To fit a profile for the actual winds to the observations, free convection scaling is assumed to govern the wind profile before the upward heat flux vanishes. The free convection scaling assumption is that turbulence in the lower part of the mixed layer is buoyantly driven (Ref. 10), and provides a relationship for the wind shear

$$\frac{\partial U}{\partial z} = bz^{-4/3} \quad (31)$$

which results in a velocity defect expression

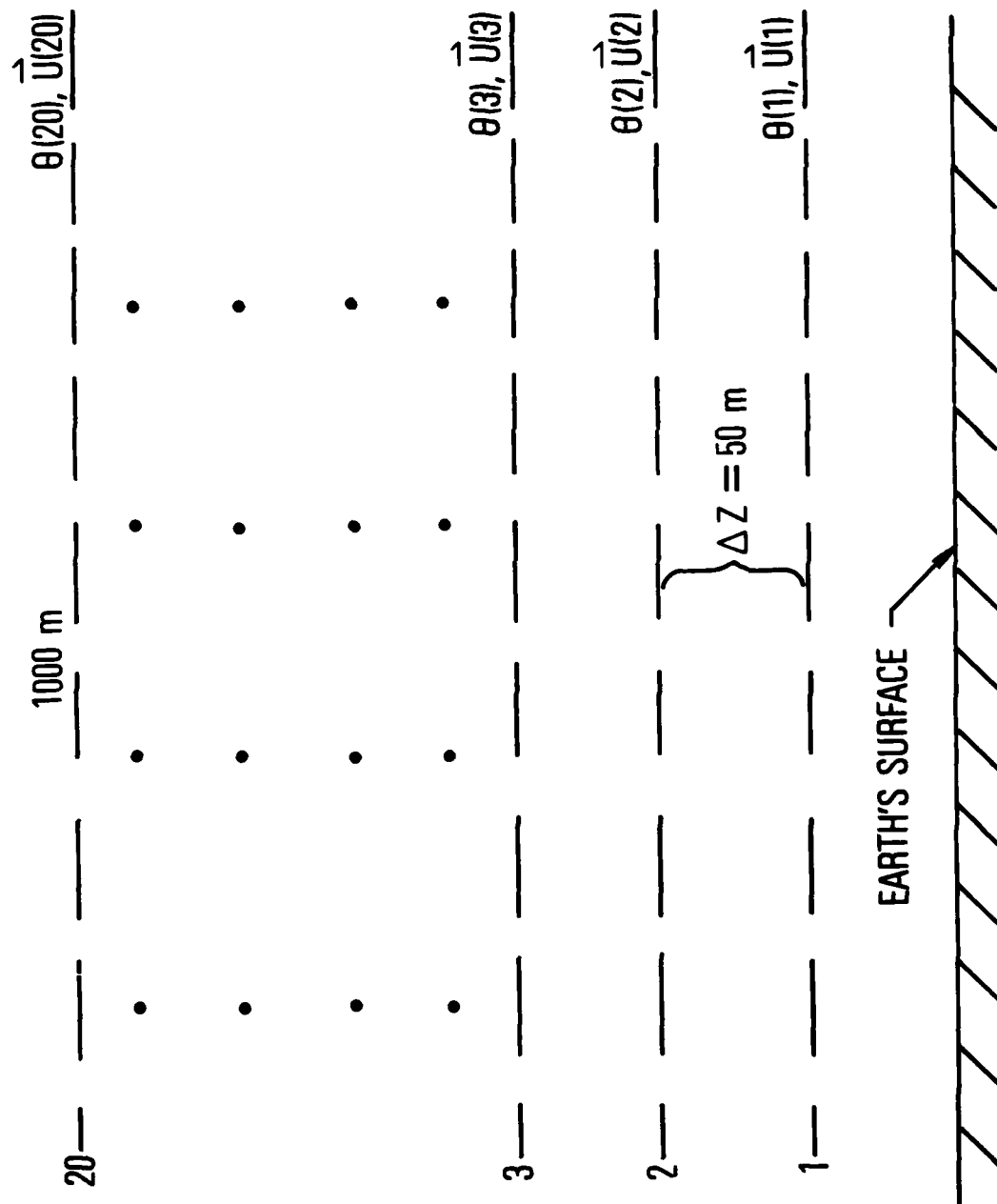


Fig. 4. Basic Structure of Nocturnal Component of Model

$$U - U_{obs} = bz^{-1/3} \quad (32)$$

where b is determined empirically and z is measured downward from z_{obs} (where $z = 0$ and $U = U_{obs}$). Equation (32) is applied to 00Z wind data for the layer between the top of the surface layer at 50 and 200 m; above 200 m the wind is assumed initially to be constant up to 1000 m. The complete form of the late afternoon wind and temperature profiles is represented in Fig. 5. The specified initial wind profile may possess a significant ageostrophic component, but the model adjusts smoothly to the transition during the first 1 or 2 hr of integration beyond the time of reversal in the sign of the heat flux, and ultimately reaches quasi-equilibrium with small accelerations.

The value of the bulk Richardson number defines three stability classifications for which events in the surface layer are different.

- | | | |
|-------|---------------|--------------|
| (I) | $B < 0$ | Unstable |
| (II) | $0 < B < 0.2$ | Stable |
| (III) | $B > 0.2$ | Nonturbulent |

In cases I and II, the surface heat flux [given by Eq. (23)] is positive when the surface layer is unstable (a situation that rarely occurs at night), and negative (downward directed) when the surface layer is stable. For case III, the surface layer is decoupled from events above 50 m because of the strongly stable lapse rate near the ground [$\theta(50 \text{ m}) > \theta_g$]; both u_* and H_0 then become zero.

A typical sequence of events near sunset would follow a progression through the three stability classifications with the surface layer, initially unstable, becoming stable (B increasing). As the ground temperature and wind shear stress decrease rapidly, the stratification decouples the surface layer from the atmosphere above. As the stress decreases and the turbulence near the ground ceases ($B > 0.2$), the wind above accelerates, increasing the vertical shear. If this shear becomes large enough, B can fall below 0.2 and permit a turbulent event to occur with a downward directed exchange of heat,

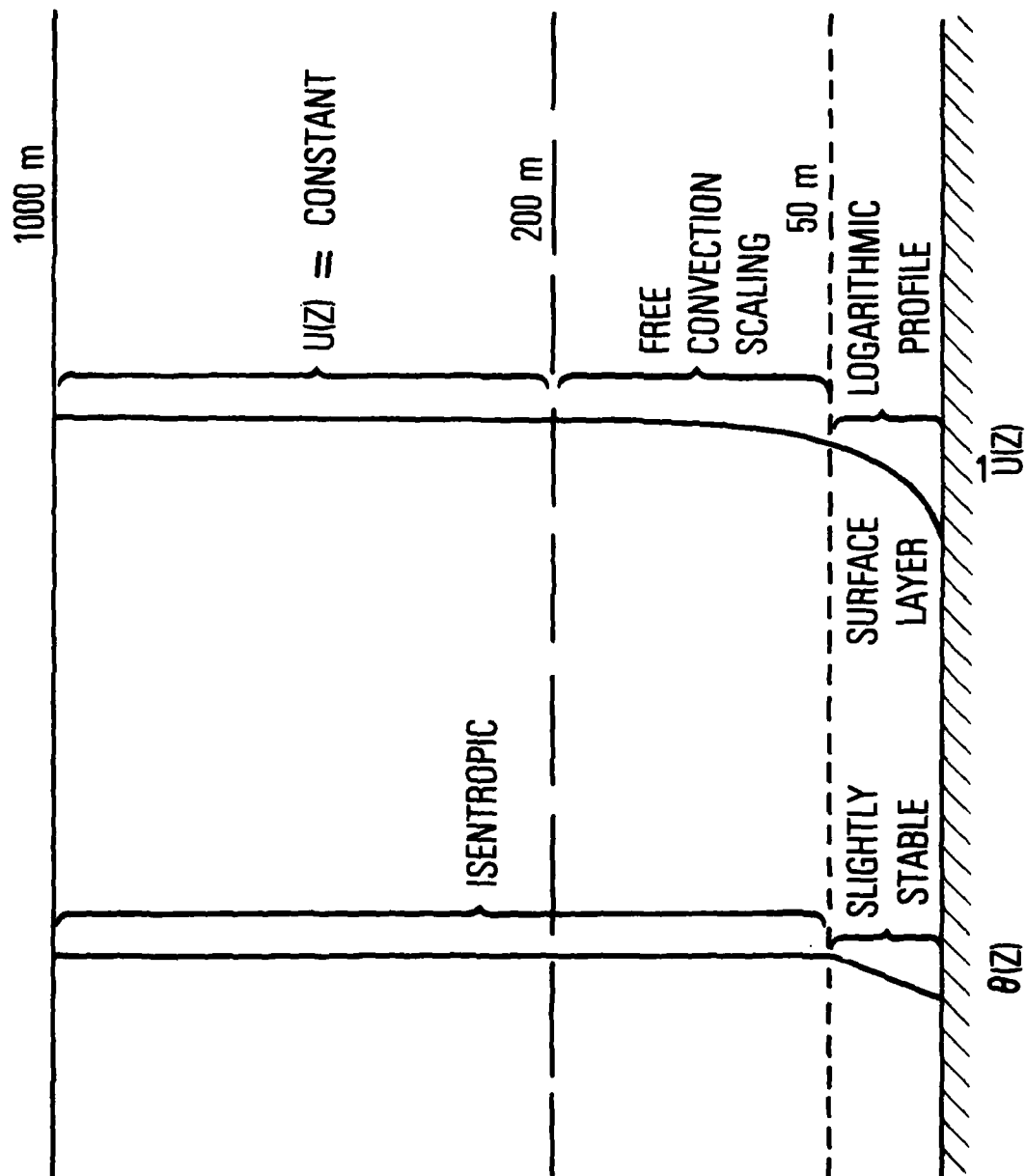


Fig. 5. Schematic of Initial Wind and Temperature Profiles for Nocturnal Component of Model

which will act to elevate the ground temperature temporarily. Such turbulence may recur throughout the night. Whereas the model will not be very accurate in timing these events, numerical tests demonstrate that this formulation successfully predicts the nights that are likely to experience turbulent episodes. The governing parameter for these events is the geostrophic wind (assumed constant with time). On nights when the surface geostrophic wind is large, turbulent events are more likely.

III. MODEL CAPABILITIES DEVELOPED AT AEROSPACE

A. DUAL-MODE CALCULATIONS

In many remote-sensing applications, it is desirable to have the capacity to simulate the thermal behavior of a relatively small target area surrounded by terrain with very different surface properties (such as thermal inertia and albedo), e.g., an asphalt road traversing an unvegetated range of sandy soil. If the target surface area is small (less than a few hundred square meters), the atmospheric properties, temperature and humidity, overlying the target would be driven by the atmospheric fluxes of the surrounding terrain rather than the temperature and humidity of the small target (except in a thin layer above the target where the eddy scale is small and horizontal advection is minimal). The atmosphere of the surrounding terrain thus influences the energy balance of the target surface; the local temperature and moisture anomalies of the target do not alter the large-scale atmospheric properties driven by the energy balance of the surrounding terrain.

This dual mode capacity has been incorporated into a version of the model (HDUAL) that, in one recent application, was effective in predicting the thermal signature of a concrete pad surrounded on all sides by a composite sand-granite soil. The target and terrain are modeled to possess separate (and often quite dissimilar) values for parameters such as thermal inertia, albedo, emissivity, and moisture availability.

B. SUBSURFACE MODEL

In its original form HFLUX used an explicit differencing scheme to model the diffusion, Eq. (13), that governs the transfer of heat through the substrate. The stability criterion for this differencing scheme limits the vertical resolution permissible in the substrate, and the thermal properties were restricted to be constant with depth. In many applications this is adequate, but in the current version of HFLUX, the former differencing method has been replaced by the implicit Crank-Nicholson scheme to permit better resolution in the substrate and allow for depth-dependent values of thermal inertia and

multiple layers (of different materials). With this procedure, it is now possible to model a complex substrate matrix, and applications that require fine resolution near the surface are easily handled. This submodel also permits the inclusion of multiple boundary conditions that are necessary in special simulations.

C. DYNAMIC UPDATING

HFLUX now has the capacity to accept dynamic updating. Meteorological field data measured at 5-min intervals have been reduced and placed on a data file. These data are read sequentially into the model at each time step and replace the customary theoretical calculations of solar insolation, atmospheric radiation, and subsurface temperature within HFLUX with actual weather station measurements. With dynamic updating, model calculations are nudged with measured field data toward the actual thermal state of the ground and atmosphere, and this results in a more accurate prediction of ground temperature and the surface energy balance. Also, the handling of atmospheric transients such as cloudiness is far superior to that of the empirical relations that would otherwise be used to simulate their presence. Tests comparing updated and nonupdated simulations on days with significant cloudiness and variable weather have conclusively demonstrated the utility of dynamic updating.

IV. FUTURE DEVELOPMENTS

A. SOIL MOISTURE

Sensitivity tests indicate that the amplitude of the ground temperature wave is most responsive to changes in the surface moisture availability and thermal inertia. The value of these parameters is closely related to the distribution of moisture in the upper layer of the soil (~ 10 cm), and the capacity to model water transport in the soil would be of great value. The rate of liquid water and water vapor movement in a soil is a strong function of the soil composition (e.g., sand and clay), and the determination of the coefficients in the transport equations that are unique to each soil type will require much more extensive field work. This constitutes a fundamental problem in the creation of a soil moisture submodel. The coefficients exist in the literature for a limited number of soils that have received attention.¹¹

Deardorff¹² has proposed a predictive equation for the surface moisture derived from the conservation equation for moisture

$$\frac{\delta W_g}{\delta t} \propto C_1 E_o - C_2 \frac{(W_g - W_2)}{\tau_1}$$

in which W_g is the surface moisture content, W_2 is the vertically averaged value of moisture over the upper 25 cm of soil, and τ_1 is the diurnal period. C_1 and C_2 are coefficients that vary with moisture content and soil type. If C_1 and C_2 were known for various soils, the variation of moisture availability with time as a function of evaporation and water transport could be calculated for a broad class of soil types. When the moisture content is known for the top 10 cm, the soil thermal properties can be determined as a function of moisture content. In a saturated soil, water fills the gaps between soil granules, increasing the bulk thermal inertia, whereas air occupies these gaps in a dry soil, which results in relatively small values for P . Pratt and Ellyett¹³ have discussed in detail the determination of thermal inertia as a function of moisture content.

A version of Deardorff's submodel soon will be included in HFLUX to simulate the behavior of the surface soil moisture and its effect on the thermal properties of the soil.

B. ENERGY BUDGET OVER WATER

Another extension of HFLUX that may prove useful in future applications will include the capacity to determine the surface energy balance over water. A current version (HPUDL) calculates the surface temperature and evaporation time scale for a small puddle of water over an asphalt surface.

C. MODEL CONSOLIDATION

A longer term objective is to construct a very generalized form of the model that would permit the simulation of thermal signatures for a complex set of terrain features such as a matrix of buildings, water bodies, vegetation, and homogeneous or natural materials, such as concrete and sand. Successive application of the model for each of the above scenes would produce a thermal image that would be very useful in scene identification and image decorrelation techniques.

REFERENCES

1. Carlson, T. N., and Boland, T., "Analysis of Urban-Rural Canopy Using a Surface Heat Flux Temperature Model," J. Appl. Met. 17, 998 (1978).
2. Tennekes, H., "A Model for the Dynamics of the Inversion Above a Convective Boundary Layer," J. Atmos. Sci. 30, 558 (1973).
3. Nappo, C. J., "Parameterization of Surface Moisture and Evaporation Rate in a Planetary Boundary Layer Model," J. Appl. Met. 14, 289 (1975).
4. Panofsky, H. A., "The Atmospheric Boundary Layer Below 150 Meters," X8058, Ann. Rev. Fluid Mech. 6, 147 (1974).
5. Manual of Remote Sensing, (American Society of Photogrammetry, Falls Church, Va., 1975).
6. Sellers, W. D., Physical Climatology, (University of Chicago Press, Chicago, 1965).
7. Blackadar, A. K., "Modeling the Nocturnal Boundary Layer," Third Symp. on Atmospheric Turbulence, Diffusion, and Air Quality, Raleigh, N. C. (1976).
8. Mellor, G. L., and Yamada, T., "A Hierarchy of Turbulence Closure Models for Planetary Boundary Layers," J. Atmos. Sci. 31, 1791 (1974).
9. Vigeant, S. A., Comparative Verification of Two Atmospheric Boundary Layer Models, M.S. Thesis, The Pennsylvania State University (1978).
10. Tennekes, H., "Free Convection in the Turbulent Ekman Layer of the Atmosphere," J. Atmos. Sci. 27, 1027 (1970).
11. Philip, J. R., "Evaporation and Moisture and Heat Fields in the Soils," J. Meteor. 14, (1957).
12. Deardorff, J. W., "Efficient Prediction of Ground Surface Temperature and Moisture, with Inclusion of a Layer of Vegetation," J. Geophys. Res. 83, 1889 (1978).
13. Pratt, D. A., and Ellyett, C. D., "The Thermal Inertia Approach to Mapping of Soil Moisture and Geology," Remote Sens. Environ. 7, 151 (1979).

LABORATORY OPERATIONS

The Laboratory Operations of The Aerospace Corporation is conducting experimental and theoretical investigations necessary for the evaluation and application of scientific advances to new military concepts and systems. Versatility and flexibility have been developed to a high degree by the laboratory personnel in dealing with the many problems encountered in the Nation's rapidly developing space systems. Expertise in the latest scientific developments is vital to the accomplishment of tasks related to these problems. The laboratories that contribute to this research are:

Aerophysics Laboratory: Aerodynamics; fluid dynamics; plasmadynamics; chemical kinetics; engineering mechanics; flight dynamics; heat transfer; high-power gas lasers, continuous and pulsed, IR, visible, UV; laser physics; laser resonator optics; laser effects and countermeasures.

Chemistry and Physics Laboratory: Atmospheric reactions and optical backgrounds; radiative transfer and atmospheric transmission; thermal and state-specific reaction rates in rocket plumes; chemical thermodynamics and propulsion chemistry; laser isotope separation; chemistry and physics of particles; space environmental and contamination effects on spacecraft materials; lubrication; surface chemistry of insulators and conductors; cathode materials; sensor materials and sensor optics; applied laser spectroscopy; atomic frequency standards; pollution and toxic materials monitoring.

Electronics Research Laboratory: Electromagnetic theory and propagation phenomena; microwave and semiconductor devices and integrated circuits; quantum electronics, lasers, and electro-optics; communication sciences, applied electronics, superconducting and electronic device physics; millimeter-wave and far-infrared technology.

Materials Sciences Laboratory: Development of new materials; composite materials; graphite and ceramics; polymeric materials; weapons effects and hardened materials; materials for electronic devices; dimensionally stable materials; chemical and structural analyses; stress corrosion; fatigue of metals.

Space Sciences Laboratory: Atmospheric and ionospheric physics, radiation from the atmosphere, density and composition of the atmosphere, aurorae and airglow; magnetospheric physics, cosmic rays, generation and propagation of plasma waves in the magnetosphere; solar physics, x-ray astronomy; the effects of nuclear explosions, magnetic storms, and solar activity on the earth's atmosphere, ionosphere, and magnetosphere; the effects of optical, electromagnetic, and particulate radiations in space on space systems.

**DA
FILM**